ISSN: 2502-2318 (Online)
ISSN: 2443-2911 (Print)
Alamat URL http://omega.uhamka.ac.id/

ω | o m e g a

Omega: Jurnal Fisika dan Pendidikan Fisika **3** (1), 15 - 22 (2017)

Grain Size Analysis on Pure and Zn-doped Ilmenite Magnesium Titanane Powders

Frida U. Ermawati[1,*], S. Suasmoro[2], Suminar Pratapa[2]

[1] *Department of Physics, Universitas Negeri Surabaya*
Kampus Ketintang, Surabaya 60231
[2] *Department of Physics, Institut Teknologi Sepuluh Nopember*
Kampus Sukolilo, Surabaya 60111

Abstract

Ilmenite structured of magnesium titanate ($MgTiO_3$)-based ceramic has been the favorite candidate for microwave frequency applications, such as in mobile and satellite communication systems, dielectric resonantor, antenna, radar and global positioning system (GPS) due to the excellent dielectric performance, *i.e.* a moderate permittivity ($\varepsilon_r \sim 17.6$) together with a high quality factor ($Q \times f$) of $\sim 33,768$ GHz at 10 GHz and a near zero temperature coefficient of the resonance frequency ($\tau_f \sim -48$ ppm/°C) (Wang, *et al.* 2012). Many efforts have been made to fabricate $MgTiO_3$-based ceramics with improved performance, including preparation of nanostructured $MgTiO_3$ powder as the ceramic precursor. Having powder with nanoscale grain size is very advantageous in the ceramic fabrication because the total surface area of contact between nanoscale grains are much larger than the similar total surface area of contact between microscale grains, and the presence of the larger surface energy in the nanopowder turns out to be a driving force of sintering; in this case, to reduce the free energy of the system during the sintering process. Sintering process is a process of firing of compact powder to produce ceramic with controlled microstructure, reduced porosity and enhanced properties. This paper reported the work to analyze the grain sizes in a series of $Mg_{1-x}Zn_xTiO_3$ for $x = 0 - 0.5$ (MZT0 - MZT0.5) powders prepared from Mg, Zn and Ti metals powders and hydrochloric acid (Merck©) using a facile wet mixing method. The Zn-doped samples were calcined at 550 °C, while that of the zinc free sample was at 700 °C. Bright field-transmission electron microscope (BF-TEM), *MAUD*-based x-ray diffraction (XRD) and particle size analyzer (PSA) analysis methods were occupied to measure the average grain sizes of the calcined powders, as well as the particle size distribution, and the results were compared. Discussion on the phase formation and thermal events during thermal treatment of the system was also provided.

Keywords: Magnesium titanate, ceramic, average grain size, TEM, *MAUD*-based XRD, PSA

*Corresponding author. E-mail address: frida.ermawati@unesa.ac.id

Introduction

Investigation on dielectric materials for microwave frequency applications has been initiated since almost three decades ago and research development on these applications has been increasing with rapid progress in mobile and satellite communication systems [1-6]. The efforts to miniaturize the microwave circuits have further boosted up the growth of wireless communication industry [7]. There are three important aspects for using a dielectric ceramic in microwave frequencies, namely a high relative permittivity (ε_r) in order to reduce the size of the components, a high quality factor ($Q \times f$) to increase the frequency selectivity, and good temperature stability (τ_f) to ensure high temperature stability [8]. Ilmenite magnesium titanate ($MgTiO_3$) ceramic with a moderate permittivity ($\varepsilon_r \sim 17.6$) together with a high quality

factor ($Q \times f$) of $\sim 33,768$ GHz at 10 GHz and a near zero temperature coefficient of the resonance frequency ($\tau_f \sim -48$ ppm/°C) [9] meets the above requirement and therefore $MgTiO_3$ has been one of the favorite candidates for microwave frequency applications. Many efforts have been carried out to fabricate $MgTiO_3$-based ceramics with improved performance, including varying powder preparation technique [10-12], improving sintering behavior by introducing a liquid phase agent as a sintering aid [13], controlling microstructure [14], developing new dielectric ceramic by combining two or more compositions with τ_f characteristic compensation, *i.e.* to adjust the τ_f value approaches to zero [15]. A study to investigate the dielectric performance of a series of developed $MgTiO_3$-based ceramic as a function of frequency (from 1 Hz to 7.7 GHz) has been carried out by the authors [16].

Powder with nanoscale grain size is very beneficial in the ceramic fabrication because the total surface area of contact between grains with nanoscale are much larger than the similar total surface area of contact between grains with microscale. The presence of the larger surface energy in the nanopowder turns out to be a driving force of sintering; in this case, to reduce the free energy of the system during the sintering process. Sintering process is a densification process of compact powder by firing the powder to produce ceramic with controlled microstructure, reduced porosity and enhanced properties, such as strength, electrical and thermal conductivities. The driving force for densification is the change in free energy from the decrease in surface area and lowering of the surface free energy by the replacement of solid-vapor interfaces [17]. This process forms new but lower-energy solid-solid interfaces with a total decrease in free energy occurring. On a microscopic scale, material transfer is affected by the change in pressure and differences in free energy across the curved surface. If the size of the particle (*i.e.* a group of grains) is very small and its curvature is high, these effects become very large in magnitude. The change in energy is much higher when the radius of curvature is less than a few micrometres, which is one of the main reasons why many ceramic technologies are based on the use of fine-particle materials.

This paper reported the analysis on the average grain sizes of a series of nanostructured $Mg_{1-x}Zn_xTiO_3$ powders for $x = 0 - 0.5$ both measured from bright field-transmission electron microscope (BF-TEM) and x-ray diffraction (XRD) study. By means of XRD study is analyzing the XRD powder spectra quantitatively using the Rietveld method implemented in *MAUD* program. XRD-based analysis is also aimed to extract the phase composition data of the samples. This particular analysis was completed using the Rietveld method implemented in *Rietica* program. Further, analysis on the particle size distribution was carried out using particle size analyzer (PSA). Such data adds the information on how many grains reside, in average, in each particle in the systems. Furthermore, analysis on the phase formation and thermal events during thermal treatment of the powders was also presented in this paper.

Experiment

The compositions of $Mg_{1-x}Zn_xTiO_3$ dried powders for $x = 0 - 0.5$ (MZT0 - MZT0.5) were synthesized from Mg, Ti and Zn metal powders (Merck©) as starting materials and hydrochloric acid as a solvent using a facile dissolved metals mixing method [11]. The use of this method, metal powders as starting materials and hydrochloric acid as the solvent are the best combination to produce high purity $MgTiO_3$ crystalline phase at quite low temperature without accompanied by undesired, intermediate phase of Mg_2TiO_4 (*qandilite*) or Mg_2TiO_5 (*karrooite*). By dissolving Mg, Ti and Zn metals powders in strong hydrochloric acid, intimate mixing between Mg^{2+}, Zn^{2+}, Ti^{4+} and Cl^- ions occurs immediately to form $MgCl_2$, $ZnCl_2$ and $TiCl_4$ liquid solutions accompanied by H_2 gas. In this work, to ensure the stoichiometry of the dried powder, purity of the starting materials were previously examined by x-ray fluorescence (XRF) spectrometer. Each metal powder was weighed according to the molar ratio Mg: Zn: Ti = $(1-x)$: (x): 1 before being dissolved separately in hydrochloric acid using a magnetic stirring hotplate. Mg and Zn powders were dissolved at room temperature, each to obtain clear yellowish $MgCl_2$ liquid and $ZnCl_2$ liquid, while Ti powder was dissolved at $60-70$°C to obtain clear purplish $TiCl_4$ liquid. All the $MgCl_2$, $ZnCl_2$ and $TiCl_4$ liquids were homogeneously mixed and the resulting liquid solution was subsequently evaporated to obtain agglomerated dried powder precursor. Agglomeration was crushed manually to obtain fine grain size powder. The fine grain size powder precursors obtained from $Mg_{1-x}Zn_xTiO_3$ with $x = 0.1 - 0.5$ were then calcined at 550 °C for 2 h at the heating rate of 10 °C/min using a Carbolite RHF-1400 furnace. The zinc-free dried powder ($x = 0$), however, was calcined at 700 °C for 2 h because in this particular composition, the formation of $MgTiO_3$ phase at 550 °C was still premature.

Crystalline phases in the calcined powders were identified by x-ray diffraction (XRD) using an XPert Diffractometer (Philips) with CuK_α radiation. The XRD measurement was carried out from $2\theta = 15$ to 65° and the step size is 0.02°. Analysis on the phase composition was performed using the Rietveld-based *Rietica* program [18]. A bright field-transmission electron microscopy (BF-TEM) image on the calcined powder was taken using FEI

type Tecnai G2 20 S-TWIN with the accelerating voltage of 200 kV and the camera length of 15 cm; and the average grain sizes were directly measured from the BF-TEM data. The TEM specimen was prepared by dispersing the powder in ethanol using an ultrasonic bath. The similar grain sizes were also estimated based on the XRD study using *MAUD* program [19] implemented in the Rietveld method. Particle size distribution in the samples was measured using particle size analyzer (PSA) Zetasizer Nano Series Software Version 7.01 (Malvern Instrument®). The PSA specimen was prepared by dispersing about 0.5 gram of the calcined powder in aquadest using ultrasonic bath. About 2-3 drops of a dispersant liquid was also added to break up the agglomerated particles.

Results and Discussion

Phase Formation and Thermal Events during Thermal Treatment

XRD spectra of MZT0.1 - MZT0.5 powders after being calcined at 550 °C and of MZT0 powder after being calcined at 700 °C both are provided in Fig. 1. In addition, Fig. 1 also shows the evolution of crystalline phases detected in MZT0.1 powder at room temperature (RT) and after being calcined subsequently at 300, 400, 450 and 500 °C. As shown, at RT, the MZT0.1 powder precursor contains peaks from $MgCl_2 \cdot 6\,H_2O$ (PDF No. 25-0515), $ZnCl_2$ (PDF No. 15-0452) at 2θ = 18.5° and TiO_2 (PDF No. 21-1276) phases. Study of the phase formation and thermal events in the MZT0.1 system carried out via thermo gravimetric and differential thermal analyses (TGA/DTA), which are not shown here, explains that from RT to 300 °C, 4 mol H_2O gas was released as a result of dehydration of about 0.9 mol $MgCl_2 \cdot 6\,H_2O$. From 300 to 400 °C, a transition of $Mg_{0.9}Zn_{0.1}Cl_2 \cdot H_2O$ to $Mg_{0.9}Zn_{0.1}(OH)Cl$ was predicted to occur following the mass loss within that temperature range. The presence of a significant endothermic peak at 400 °C suggested that the formation of $Mg_{0.9}Zn_{0.1}TiO_3$ crystalline phase was initiated at that temperature, and the mass loss within the range of 400 − 500 °C was addressed to the emission of 1 mol HCl gas from $Mg_{0.9}Zn_{0.1}(OH)Cl$. The later phase was then reacted with TiO_2 to produce $Mg_{0.9}Zn_{0.1}TiO_3$ phase. This phase can be indexed as $MgTiO_3$ with PDF No. 06-0494 (see the spectrum labeled 'MZT0.1_500', *i.e.* the peaks with *hkl* indices in Fig.1).

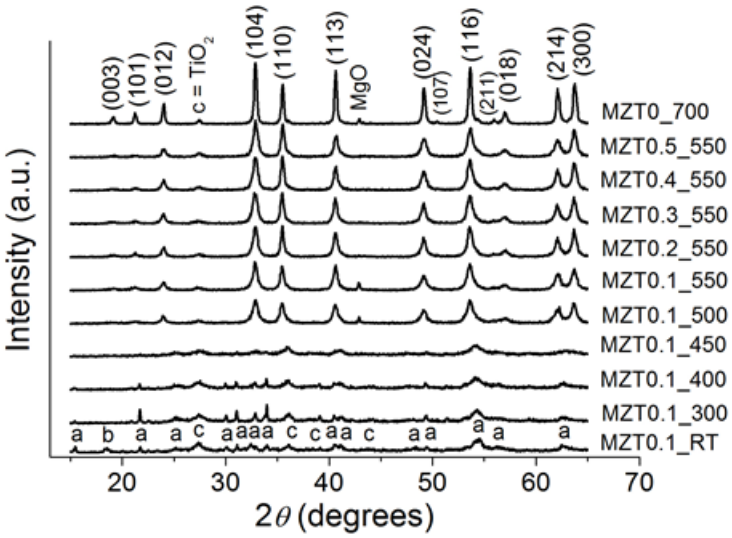

Fig. 1: XRD spectra of MZT0.1 - MZT0.5 powders after being calcined at 550 °C and of MZT0 calcined at 700 °C, each for 2 h. Evolution of the crystalline phases detected in MZT0.1 powder both at room temperature (RT), and after being calcined at 300, 400, 450, and 500 °C are also shown. The indexed peaks = $MgTiO_3$, a = $MgCl_2 \cdot 6\,H_2O$, b = $ZnCl_2$ and c = TiO_2.

In addition, as also seen in the spectrum labeled 'MZT0.1_RT' in Fig. 1, the $ZnCl_2$ peak at 2θ = 18.5°(labeled 'b') totally disappeared when the powder was heated. This fact suggested that Zn-ion substitution into the $MgCl_2 \cdot 6\,H_2O$ structure, *i.e.* $(Mg_{1-x}Zn_x)Cl_2 \cdot 6\,H_2O$, was started after heating. This $(Mg_{1-x}Zn_x)Cl_2 \cdot 6\,H_2O$ substitution is feasible due to the ionic radius similarity found in Mg and Zn-ions, *i.e.* 0.074 nm for Zn and 0.072 nm for Mg, respectively. This substitution is an early indication on the formation of solid solution phase in MZT0.1 system. The formation of such solid solution phase is also confirmed by the absence of peaks containing zinc in all spectra in Fig. 1, *i.e.* in the 'MZT0.1_550', 'MZT0.2_550', 'MZT0.3_550', 'MZT0.4_550' and 'MZT0.5_550' spectra. Despite the fact that the desired $Mg_{0.9}Zn_{0.1}TiO_3$ phase has been formed in the system at 500 °C, however, cal-

cination of MZT0.1 - MZT0.5 powders was carried out at 550 °C for 2 h because, as has been reported in [11], calcination at 550 °C yielded the most optimum molar fraction of the desired phase. For the zinc-free sample (MZT0), however, calcination was carried out at 700 °C for 2 h and this calcination temperature also provides the main $MgTiO_3$ phase, but the presence is accompanied by a minor TiO_2 peak at $2\theta = 27.5°$ and an MgO (PDF No. 45-0946) peak at $2\theta = 42.5°$ (see the spectrum labeled 'MZT0_700' in Fig. 1).

Phase Composition Analysis using Rietveld-based *Rietica*

Figure 2 provides the Rietveld refinement on the spectral model (generated from $MgTiO_3$ phase (PDF No. 06-0494) and TiO_2 phase (PDF No. 21-1276) in the *Rietica* program) with respect to the 'MZT0.2_550' spectrum in Fig. 1. The refinement result on the 'MZT0.2_550' spectrum is shown here as a representative of the similar refinements performed to the other spectra, *i.e.* the 'MZT0_700', 'MZT0.1_550', 'MZT0.3_550', 'MZT0.4_550' and 'MZT0.5_550' spectra. The label '+' in Fig. 2 indicates the experimental spectrum, the red line assigns the spectral model, the green line shows the difference between the model and the experimental spectra, while the blue vertical lines underneath the spectra represent the position of Bragg peaks for the two identified phases, $MgTiO_3$ and TiO_2. As observed, all the Bragg peaks coincide with the experimental peaks indicating that all peaks/phases were well identified. In other words, other than the two identified $Mg_{0.8}Zn_{0.2}TiO_3$ and TiO_2 phases, there is no extra phase coexists in the 'MZT0.2_550' samples. As also seen, the difference between the experimental and the model spectra especially at $2\theta = 32.9$ and 35.5° are significant. This difference, however, does not significantly alter the refinement result. Table 1 recapitulates the output of the refinement carried out for all the samples, covering the identified phases, the lattice parameters, the unit cell volumes, the molar phase percentage and the theoretical density data. Figure-of-merit (*FoM*) values of the refinements are also shown. The values are acceptable and therefore the data in Table 1 can be used for further analysis.

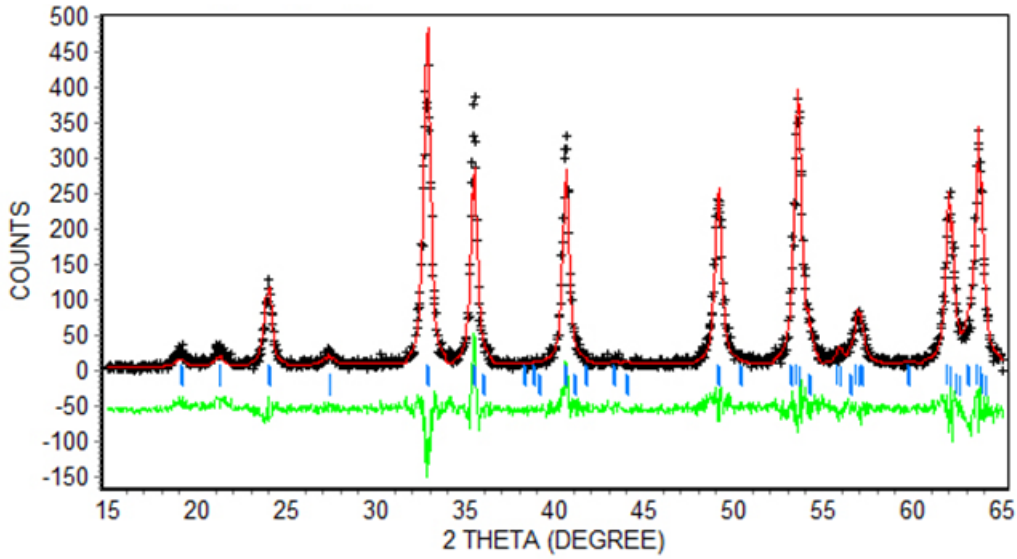

Fig. 2: The Rietveld refinement on the spectral model (red line) with respect to the experimental XRD spectrum ('+') of MZT0.2 powder calcined at 550 °C in Fig. 1 using *Rietica* program. Figure-of-Merit (*FoM*) of the refinement is $R_{wp} = 17.2$; $R_p = 13.9$; $R_{exp} = 12.3$ dan $GoF = 2.0$.

As seen in Table 1, $MgTiO_3$ phase and its solid solution phase ($Mg_{1-x}Zn_xTiO_3$) are identified as the main phase in all samples. These are assigned by the presence of the main phase in very significant molar percentage, namely (93.0 ± 3.0) % in MZT0, (97.9 ± 3.0) % in MZT0.1, (98.5 ± 4.0) % in MZT0.2, (97.2 ± 2.9) % in MZT0.3, (95.9 ± 2.0) % in MZT0.4 and (95.5 ± 1.9) % in MZT0.5, respectively. The remaining molar percentages belong to the minor phases, *i.e.* TiO_2 and MgO in MZT0 and MZT0.1 samples and TiO_2 in MZT0.2 - MZT0.5 samples. In terms of the lattice parameters of the main phase, the values of both 'a' and 'c' parameters increase slightly with the zinc content, namely for the 'a' parameter = 5.059 Å in MZT0, 5.062 Å in MZT0.1, 5.062 Å in MZT0.2, 5.063 Å in MZT0.3, 5.066 Å in MZT0.4 and 5.067 Å in MZT0.5. The increase for the 'c' parameter are 13.901 Å in MZT0, 13.904 Å in MZT0.1, 13.903 Å in MZT0.2, 13.905 Å in MZT0.3, 13.907 Å in MZT0.4 and 13.910 Å in MZT0.5. The similar increase is also recorded in the unit cell volume data (in $Å^3$), namely (308.8 ± 0.5) in MZT0,

(309.1 ± 0.6) in MZT0.1, (309.2 ± 0.5) in MZT0.2, (309.7±0.5) in MZT0.3, (310.0±0.6) in MZT0.4 and (310.3 ± 0.6) in MZT0.5. These increases confirm the analysis given previously in Sub Section 3.1 that the main phases in MZT0.1 - MZT0.5 samples are indeed the $Mg_{1-x}Zn_xTiO_3$ solid solution phases. In other words, the zinc ions and its content (*i.e.* the x-values in $Mg_{1-x}Zn_xTiO_3$) have positioned themselves in the $MgTiO_3$ structure. The theoretical density data in Table 1 also increases slightly; these data were calculated by *Rietica* based on the lattice parameters and chemical composition of particular sample.

Table 1: The Rietveld refinement output using *Rietica* for MZT0_700 and (MZT0.1 - MZT0.5)_550 spectra in Fig. 1

Sample	*FoM* (%)		Identified phases	Lattice parameters (Å)		Unit cell volume (Å^3)	Molar phases (%)	Theoretical density (g·cm^{-3})
MZT0	R_{wp}	16.9	$MgTiO_3$	a=b	5.059	308.8 ± 0.5	93.0 ± 3.0	4.0
	R_p	13.2		c	13.901			
	R_{exp}	8.7	TiO_2	a=b	4.601	62.8 ± 0.2	2.5 ± 0.3	4.1
	GoF	2.1		c	2.963			
			MgO	a	4.210	75.0 ± 0.3	4.5 ± 1.0	3.4
MZT0.1	R_{wp}	15.2	$Mg_{0.9}Zn_{0.1}TiO_3$	a=b	5.062	309.1 ± 0.6	97.9 ± 3.0	4.1
	R_p	11.8		c	13.904			
	R_{exp}	8.6	TiO_2	a=b	4.602	62.9 ± 0.2	1.1 ± 0.1	4.2
	GoF	1.9		c	2.964			
			MgO	a	4.209	75.1 ± 0.3	1.0 ± 0.1	3.4
MZT0.2	R_{wp}	17.2	$Mg_{0.8}Zn_{0.2}TiO_3$	a=b	5.062	309.2 ± 0.5	98.5 ± 4.0	4.1
	R_p	13.9		c	13.903			
	R_{exp}	12.3	TiO_2	a=b	4.603	63.0 ± 0.2	1.5 ± 0.7	4.2
	GoF	2.0		c	2.964			
MZT0.3	R_{wp}	17.3	$Mg_{0.7}Zn_{0.3}TiO_3$	a=b	5.063	309.7 ± 0.5	97.2 ± 2.9	4.1
	R_p	13.7		c	13.905			
	R_{exp}	8.6	TiO_2	a=b	4.604	63.1 ± 0.2	2.8 ± 0.4	4.2
	GoF	2.1		c	2.965			
MZT0.4	R_{wp}	17.9	$Mg_{0.6}Zn_{0.4}TiO_3$	a=b	5.066	310.0 ± 0.6	95.9 ± 2.0	4.2
	R_p	13.9		c	13.907			
	R_{exp}	9.2	TiO_2	a=b	4.605	63.2 ± 0.2	4.1 ± 1.0	4.2
	GoF	2.0		c	2.965			
MZT0.5	R_{wp}	17.3	$Mg_{0.5}Zn_{0.5}TiO_3$	a=b	5.067	310.3 ± 0.6	95.5 ± 1.9	4.3
	R_p	15.6		c	13.910			
	R_{exp}	9.0	TiO_2	a=b	4.604	63.3 ± 0.2	4.5 ± 1.2	4.2
	GoF	1.9		c	2.966			

Average Grain Size and Particle Size Distribution Analyses

Figure 3A shows a bright field TEM image of the MZT0.2 calcined powder and the grains morphology. In this work, BF-TEM image was only taken from MZT0.2 sample. One of the reasons is because the width of the main peak (at $2\theta = 32.9°$) in 'MZT0.2_550' spectrum in Fig. 1 is similar to the width of the main peaks at the same 2θ position in the other samples which indicates that the grain sizes in those samples are presumably also similar. As observed in Fig. 3A, morphology of the individual grains is circular or elongated in one direction; most of the grains, however, are agglomerated. Diameter of the individual grains varies from $20 - 80$ nm. As a comparison, Fig. 3B provides an estimate on the grain size distribution in MZT0.1 - MZT0.5 powders (calcined at 550 °C) and in MZT0 (calcined at 700 °C) obtained from the XRD study, *i.e.* from the output of the Rietveld refinement using *MAUD* program on the MZT0 - MZT0.5 spectra in Fig. 1. As seen, peak of the grain size distribution curve in MZT0.2 is located at 17 nm. The curve subsequently drops significantly up to 75 nm. The area under the curve estimates the range of the majority grain sizes in the sample; in the MZT0.2 case, the estimate is quite relevant to the TEM data in Fig. 3A (*i.e.* the individual grain size is up to 80 nm). The grain size distribution curves found in MZT0.1, MZT0.3, MZT0.4 and MZT0.5 powders in Fig. 3B are similar to the distribution curve in MZT0.2, suggesting that the range of the majority grain sizes, hence the average grain size, in the former mentioned powders are also similar to the average grain size in later mentioned (MZT0.2) powder.

The grain size distribution curve in MZT0 powder (also in Fig. 3B), however, is the widest among the other distribution curves. Peak of the MZT0 curve is located at 120 nm. This particular distribution curve is plausible since MZT0 powder was calcined at higher temperature (700 °C); this higher calcination temperature leads to growing of the grain size in the system. Referring back to the 'MZT0_700' spectrum in Fig. 1, it is clear that the width of the main peak at $2\theta = 32.9°$ is smaller than the width of the main peak at the same 2θ position in the other spectra, which means that the

grain size in the system is also smaller. The fact that the average grain sizes in the powders containing zinc are smaller than the average grain size in the zinc-free powder confirms that zinc substitution in the $MgTiO_3$ structure has lowered the temperature of formation of the main $MgTiO_3$ phase in the systems; this in turns results in nanoscale grain size. As verification, Fig. 4 shows the Rietveld refinement using *MAUD*, especially for the case of MZT0.2 spectrum. The symbols used in this particular refinement (using *MAUD*) have similar meanings as the symbols used in the refinement using *Rietica* in Fig. 2. As seen in Fig. 4, all the Bragg peaks (the small vertical bars underneath the spectra) also coincide with the experimental peaks suggesting that all peaks/phases were well identified.

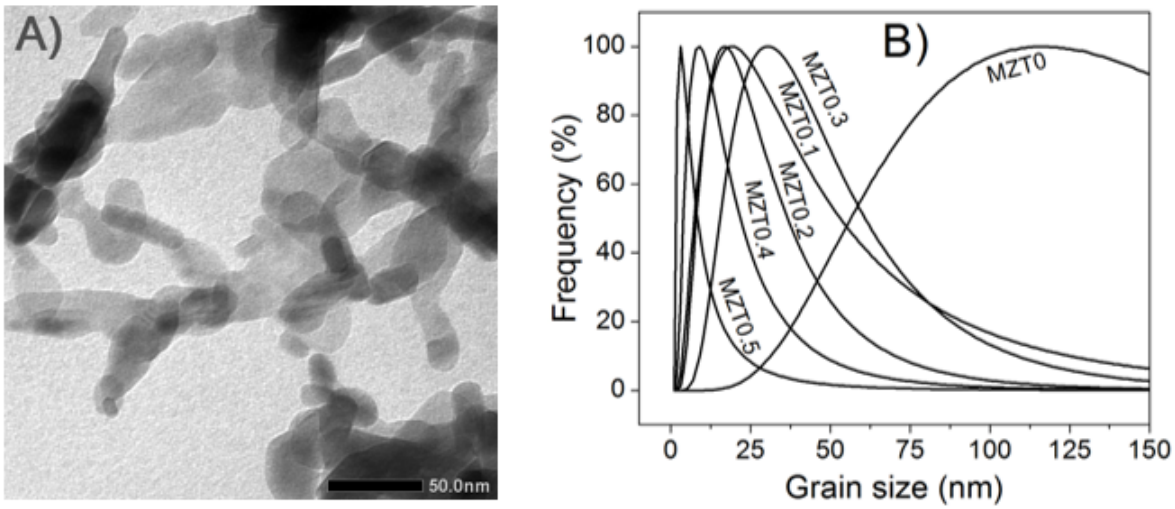

Fig. 3: A) Bright field TEM image of MZT0.2 powder after being calcined at 550 °C for 2 h. B) *MAUD*-based XRD grain sizes of MZT0.1 - MZT0.5 powders after being calcined at 550 °C for 2 h and of MZT0 powder calcined at 700 °C for 2 h.

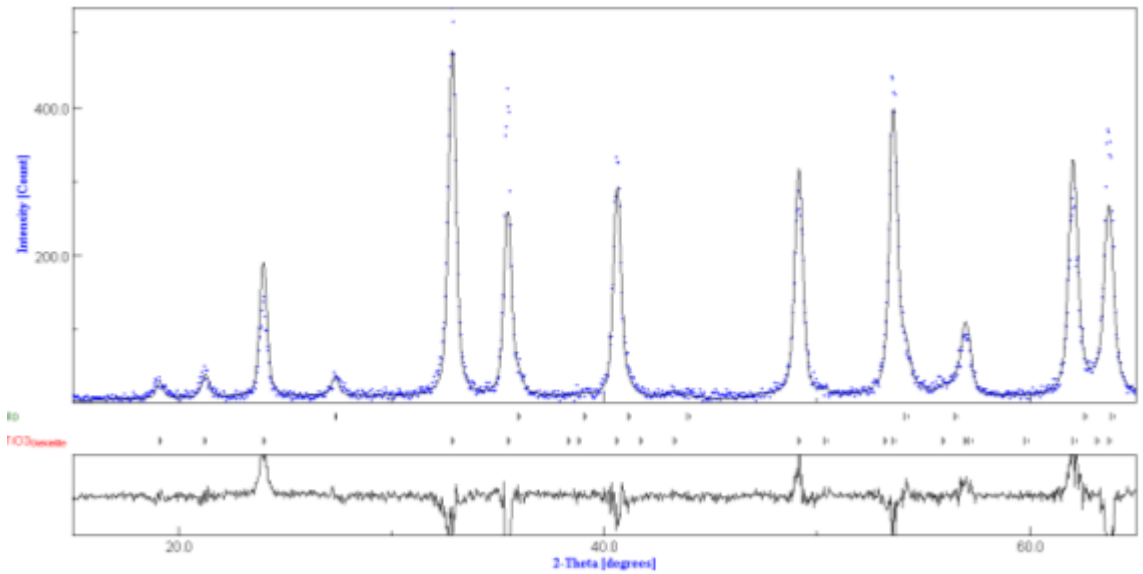

Fig. 4: The Rietveld refinement on 'MZT0.2_550' spectrum in Fig. 1 using *MAUD*. *FoM: sig* = 1.5 % and R_w = 13.7 %.

The distribution curves of particle size in MZT0 - MZT0.5 calcined powders measured using PSA are provided in Fig. 5. As observed, all distributions are a log-normal single-mode ranging from (91 − 459) nm in MZT0, (106 − 531) nm in MZT0.1, (59−712) nm in MZT0.2, (106−615) nm in MZT0.3, (79 − 700) in MZT0.4 and (91 − 530) nm in MZT0.5. The average particle size is (189 nm ± 1 %) in MZT0, (257 nm ± 3 %) in MZT0.1, (203 nm ± 5 %) in MZT0.2, (245 nm ± 5 %) in MZT0.3, (227 nm ± 5 %) in MZT0.4 and (212 nm ± 4 %) in MZT0.5. Based on the fact that the distribution curves are single modes and the deviations of the average size are diminutive, we concluded that the particles in the above samples are homogeneously distributed. Comparing the average grain size data

both obtained from TEM in Fig. 3A and *MAUD*-based XRD in Fig. 3B, as well as the distribution particle size data in Fig. 5, it can be concluded that each particle in MZT0 powder contains approximately 2 grains, in MZT0.1 contains 10 grains, in MZT0.2 contains 12 grains, in MZT0.3 contains 8 grains, in MZT0.4 contains 20 grains and finally in MZT0.5 contains 38 grains.

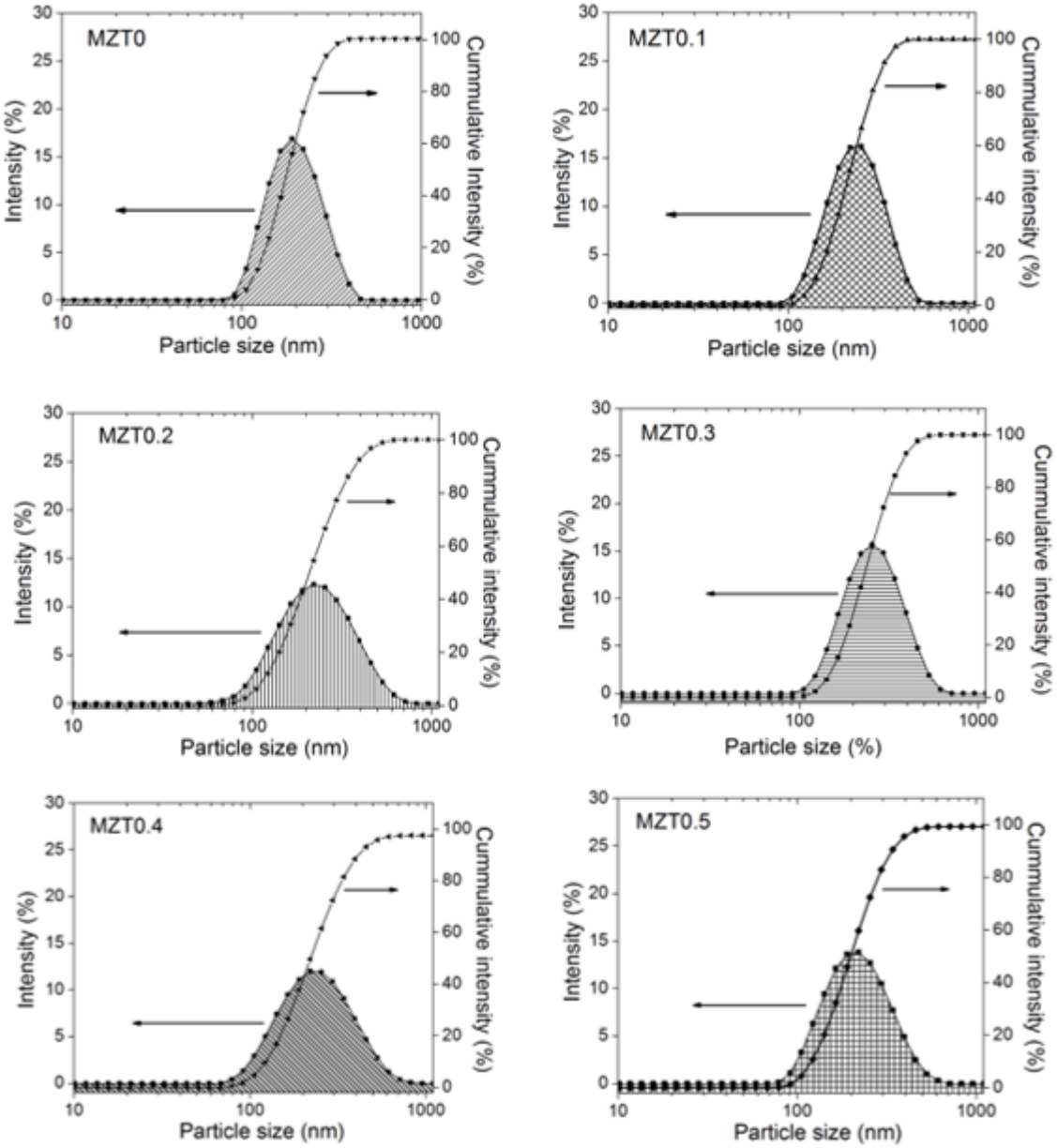

Fig. 5: Particle size distribution in MZT0 - MZT0.5 calcined powders measured using particle size analyzer (PSA) Zetasizer Nano Series Software Version 7.01 (Malvern Instrument®).

Conclusion

Study on the average grain size and particle size distribution in the series of ilmenite structured $Mg_{1-x}Zn_xTiO_3$ calcined powders for $x = 0 - 0.5$ have been carried out. The powders have nanoscale grain sizes and uniformly distribution of the particle sizes; these all are due to the facile wet mixing synthesis method. The grain sizes estimate made in *MAUD*-based XRD analysis are in good agreement with the data measured directly from bright field-transmission electron microscope (TEM). Data on the particle size distribution measured using PSA supplied the important information on the number of grains per particle. This work, therefore, has shown the comparability between TEM and *MAUD*-based XRD grain size analyses. Having such powders, the densification process of compact nanopowder via sintering, as the important part of ceramic fabrication, will be straight forward and the desired relative density will also be easily achieved.

References

[1] G. Pfaff, Ceram. Int. **20** (2), 111-116 (1994).

[2] B.A. Wechsler and R.B. von Dreele, Acta Crystallographica. Sec. B, Struc. Sci. **45** (6), 542-549 (1989).

[3] V.M. Ferreira and J.L. Baptisa, Mater. Res. Bull. **29** (10), 1017-1023 (1994).

[4] V. Parvanova and M. Maneva, Thermochim. Acta **279**, 137-141 (1996).

[5] J.F. Liao and M. Senna, Mater. Res. Bull. **30**, 385-392 (1995).

[6] I.R. Abothu, A.V. Prasada Rao, and S. Komarneni, Mater. Lett. **38** (3), 186-189 (1999).

[7] J.J. Bian, L. Wang, and L.L. Yuan, Mater. Sci. Eng. B **164** (2), 96-100 (2009).

[8] C.L. Huang, J.J. Wang, and Y.P. Chang, J. Am. Ceram. Soc. **90** (3), 858-862 (2007).

[9] H. Wang *et al.*, J. Mater. Sci. Technol. **28** (8), 751-755 (2012).

[10] B. Tang *et al.*, J. Mater. Sci. Mater. El. **25** (6), 2482-2486 (2014).

[11] F.U. Ermawati, S. Suasmoro, and S. Pratapa, Adv. Mater. Res. **1112**, 47-52 (2015).

[12] X. Xue, H. Yu, and G. Xu, J. Mater. Sci. Mater. El. **24** (4), 1287-1291 (2013).

[13] H.T. Wu *et al.*, J. Electron. Mater. **42** (3), 445-451 (2013).

[14] S.R. Kiran *et al.*, J. Am. Ceram. Soc. **95** (6), 1973-1979 (2012).

[15] C.L. Pan *et al.*, J. Alloy. Compd. **503** (2), 365-369 (2010).

[16] F.U. Ermawati *et al.*, J. Mater. Sci. Mater. El. **27** (7), 6637-6645 (2016).

[17] M.N. Rahaman, *Ceramic Processing and Sintering*, 2nd Ed. (CRC Press, Taylor & Francis Group, New York, 2003).

[18] B. Hunter, *Rietica - A Visual Rietveld Program*, WWW Document, (http://www.mx.iucr.org/iucr-top/comm/cpd/Newsletters/no20summer1998/art15/art15.htm).

[19] L. Lutteroti, *MAUD: Material Analysis using Diffraction*, WWW Document, (http://www.ing.unitn.it/∼maud.)